Pressure-induced Optical Transitions in Metal Nanoclusters

Qi Li[1], Martín A. Mosquera[2], Leighton O. Jones[2], Abhinav Parakh[3], Jinsong Chai[4], Rongchao Jin[4], George C. Schatz[2], X. Wendy Gu[1]*

[1]Department of Mechanical Engineering, Stanford University, Stanford, CA 94305, United States

[2]Department of Chemistry, Northwestern University, Evanston, IL 60208, United States

[3]Department of Materials Science & Engineering, Stanford University, Stanford, CA 94305, United States

[4]Department of Chemistry, Carnegie Mellon University, Pittsburgh, PA 15213, United States

*Corresponding author: xwgu@stanford.edu

Abstract Currently, a comprehensive understanding of the relationship between atomic structures and optical properties of ultrasmall metal nanoclusters with diameters between 1 and 3 nm is lacking. To address this challenge, it is necessary to develop tools for perturbing the atomic structure and modulating the optical properties of metal nanoclusters beyond what can be achieved using synthetic chemistry. Here, we present a systematic high-pressure study on a series of atomically precise ligand-protected metal nanoclusters. A diamond anvil cell is used as a high-pressure chamber to gradually compress the metal nanoclusters, while their optical properties are monitored *in-situ*. Our experimental results show that the photoluminescence (PL) of these nanoclusters is enhanced by up to two orders of magnitude at pressures up to 7 GPa. The absorption onset red-shifts with increasing pressure up to ~12 GPa. Density functional theory calculations reveal that the red-shift arises because of narrowing of the spacing between discrete energy levels of the cluster due to delocalization of the core electrons to the carbon ligands. The pressure-induced PL enhancement is ascribed to i) the enhancement of the near-band-edge transition strength, ii) suppression of the non-radiative vibrations and iii) hinderance of the excited-state structural distortions. Overall, our results demonstrate that high pressure is an effective tool for modulating the optical properties and improving the luminescence brightness of metal nanoclusters. The insights into structure-property relations obtained here also contribute to the rational design of metal nanoclusters for various optical applications.

Keywords: high pressure, metal nanocluster, luminescence enhancement, optical transition, diamond anvil cell

Gold and silver nanoclusters of ~200 or fewer metal atoms and surrounding ligands have fascinating, and as yet incompletely understood behavior. For instance, these nanoclusters are non-metallic in nature,[1–3] exhibit quantized energy levels with multiple overlapped absorption bands,[1,4–9] and emit near-infrared photoluminescence (PL).[10–14] These properties are in contrast to the metallic nature of larger, plasmonic gold and silver nanoparticles.[15,16] Recent research advances have enabled the synthesis of atomically precise metal nanoclusters,[17] with atomic structures that are completely solved by single-crystal X-ray diffraction analysis.[1,18–21] However, several fundamental scientific issues regarding the relationship between atomic structure, electronic structure and optical properties of metal nanoclusters remain unsolved.[1,19,22] For example, it is unclear which electronic transitions correspond to the multiple overlapped absorption bands and the abnormal long absorption "tail" characteristic of certain nanoclusters.[23,24] In addition, the PL quantum yield of many metal nanoclusters are very low and the origin of nanocluster PL is still under debate.[1,3] A large Stokes shift and long lifetimes may indicate the absorption and PL arise from different underlying states (*e.g.* singlet *vs* triplet, local state *vs* charger-transfer state),[23] but this has not been verified in many metal nanoclusters. In addition, it remains mysterious how small changes in atomic structure (*e.g.* replacing two surface gold atoms[25,26]) can drastically change the properties of metal nanoclusters. These issues hamper the ability to tailor the optical and electronic properties of metal nanoclusters for use in sensing, photo-catalysis and other applications.

These questions can be resolved by varying atomic structure (*e.g.* bond length, bond angle, and connectivity) and observing the resulting changes in electronic and optical properties (*e.g.* energy gap, oscillator strength, and electron-phonon coupling of the optical transitions), but this has been challenging to achieve using existing synthetic tools. Here, pressure is used to gradually modify the atomic structure of nanoclusters, with a level of control that cannot be achieved through synthetic chemistry. This high-pressure method is combined with *in-situ* optical spectroscopy and density functional theory (DFT) to reveal the structural origin and underlying electronic transitions associated with the optical phenomena. High-pressure techniques[27,28] have previously been used to understand the photo-physics of semiconductor (*e.g.* Si,[29,30] WS_2,[31] InP,[32] and perovskites[33–36]) and metallic nanomaterials,[37–40] but the pressure-induced electronic structure and optical properties of nanoclusters cannot be inferred from these larger nanomaterials.

Scheme 1 shows the high-pressure diamond anvil cell (DAC) compression and *in-situ* optical spectroscopy of the nanoclusters $[Au_{21}(SR)_{12}(dppm)_2]^+$ (SR = cyclohexanethiolate; dppm = bisdiphenylphosphinemethane),[25] Au_{28}(S-TBBT)$_{20}$ (S-TBBT=*tert*-butyl-benzenethiolate),[24] and $Ag_{28}Pt_1$(S-Adm)$_{18}$(PPh_3)$_4$ (S–Adm = 1-adamantanethiolate, PPh_3 = triphenylphosphine).[23] These are three representative gold and bimetallic *fcc* nanoclusters with mono-cuboctahedral and bi-cuboctahedral kernel structures. The bi-tetrahedral nanoclusters Au_{24}(S-TBBM)$_{20}$[41] (S-TBBM=4-tertbutylphenylmethancan)

and $Au_{14}Cd_1(S\text{-}Adm)_{12}$[42] (S-Adm = 1-adamantanethiol) were also investigated, and their response was compared to that of the fcc nanoclusters. DFT calculations are performed on the Au_{21} cluster to directly compute the electronic structure corresponding to pressure-induced structural changes and achieve mechanistic insight into optical transitions.

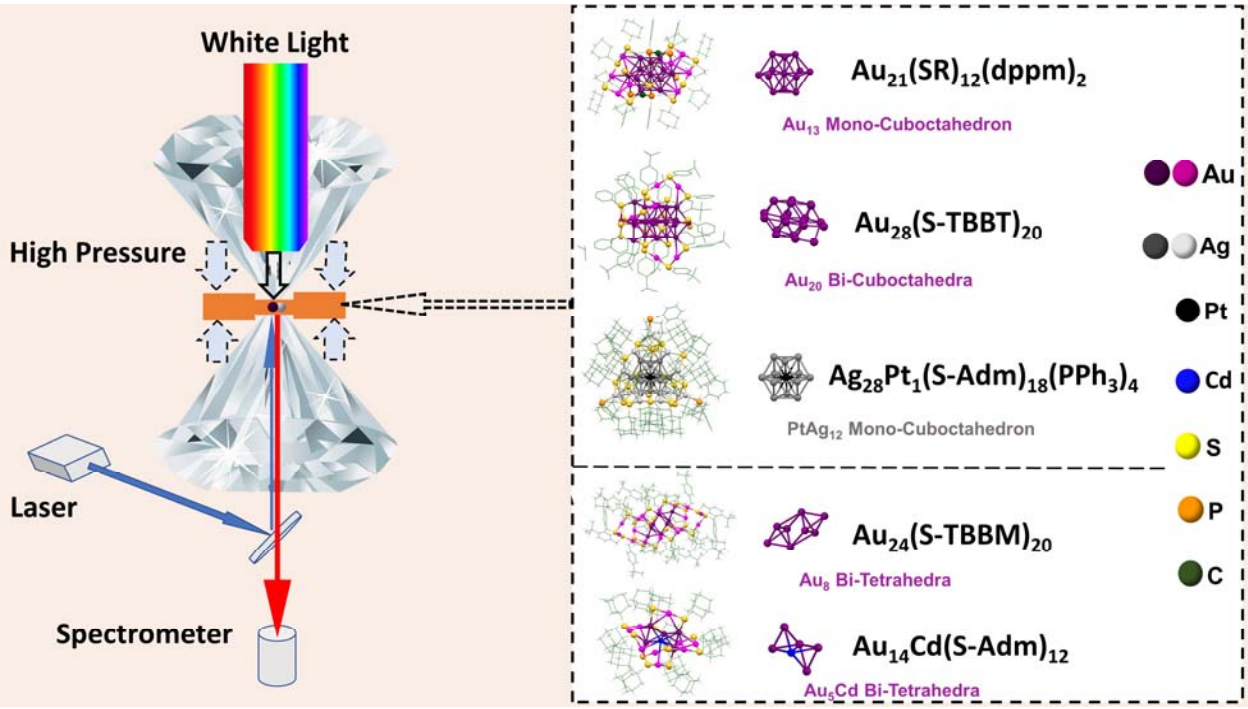

Scheme 1. Optical properties of metal nanoclusters at high pressure. Left: Schematic diagram of high-pressure compression and optical spectroscopy of nanoclusters inside a diamond anvil cell. Right: Atomic structures of $Au_{21}(SR)_{12}(dppm)_2$ (a mono-cuboctahedral Au_{13} kernel), $Au_{28}(S\text{-}TBBT)_{20}$ (bi-cuboctahedral Au_{20} kernel), $Ag_{28}Pt_1(S\text{-}Adm)_{18}(PPh_3)_4$ ($Ag_{12}Pt$ mono-cuboctahedral kernel), $Au_{24}(S\text{-}TBBM)_{20}$ (Au_8 bi-tetrahedral kernel) and $Au_{14}Cd_1(S\text{-}Adm)_{12}$ (Au_5Cd bi-tetrahedral kernel). Atomic structures are obtained from single-crystal X-ray diffraction.[23–25,41,42]

Results and Discussion

fcc nanoclusters

The pressure-dependent optical absorption and PL spectra were obtained for $Au_{21}(SR)_{12}(dppm)_2$ (Au_{21} for short hereafter) and are shown in **Figure 1**. Toluene was used as a pressure medium for Au_{21} and the other nanoclusters, as the nanoclusters are soluble in toluene. The atomic structure of Au_{21}, which has previously been solved by single-crystal X-ray diffraction,[25] is shown in Scheme 1. At ambient pressure, Au_{21} shows an intense and broad absorption peak at ~570 nm with a broad PL at ~750 nm (Figure S1). At elevated pressures of up to 9 GPa, the major absorption peak and the onset of absorption gradually red-shifts to longer wavelengths (Figure 1A). At even higher pressures (>10 GPa), the absorption peak becomes faint and no longer red-shifts. After the pressure is released back to 0.22 GPa,

the absorption peak blue-shifts to its original value of 570 nm. This indicates that the Au_{21} nanoclusters recover their original structure after pressure cycling, and do not experience permanent deformation.

The pressure-dependent PL spectra of Au_{21} are shown in Figure 1B. As with absorption, the PL of Au_{21} red-shifts with increasing pressure. The intensity of the PL first increases with increasing pressure up to ~5 GPa. The PL intensity decreases at higher pressures. This is a similar trend as the near-band-edge absorption. The increase of PL intensity below ~2 GPa has a contribution from the freezing of the toluene pressure medium at ~2 GPa[43] which suppresses structural vibrations that lead to non-radiative processes, but this does not account for the intensity increase up to ~5 GPa. The inset of Figure 1B depicts the peak wavelength of the absorption and PL of Au_{21} at different pressures, both of which show a red-shift with increasing pressure. These results suggest that the underlying electronic states for the absorption at ~570 nm and PL at ~750 nm in Au_{21} are the same.

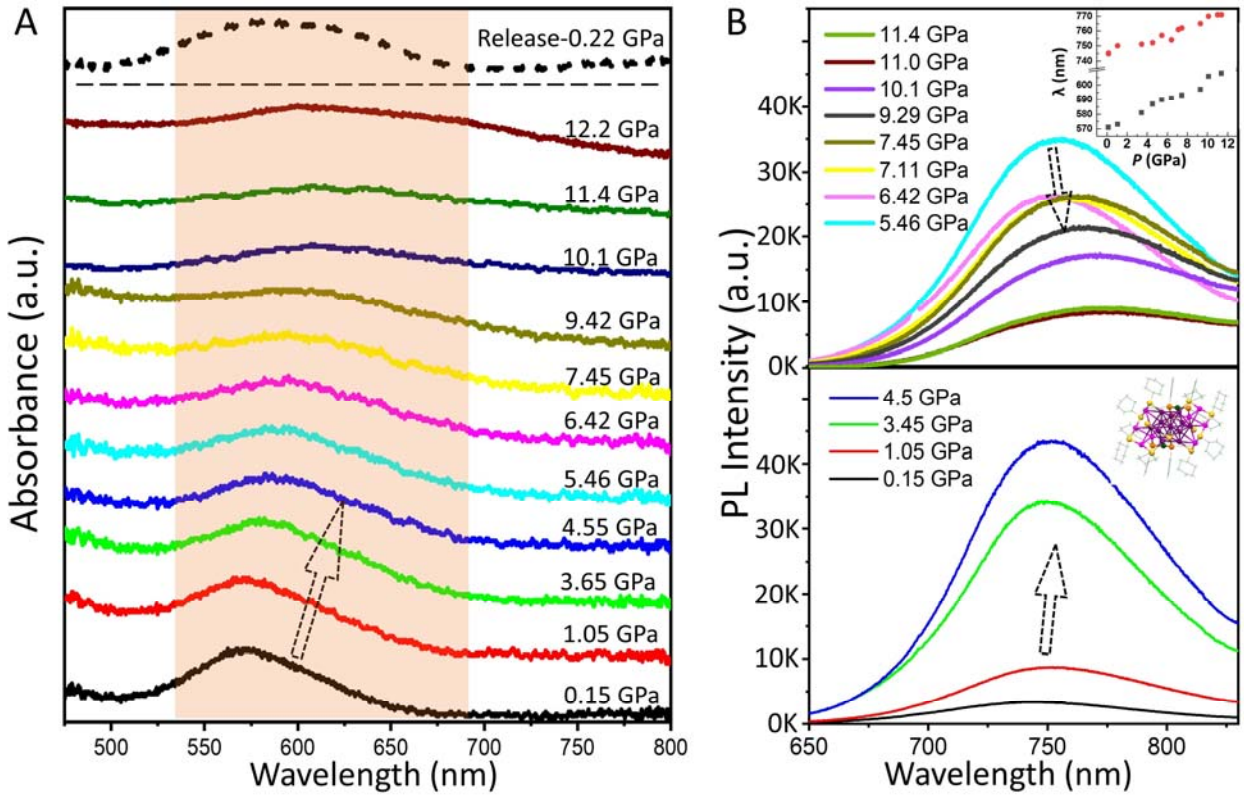

Figure 1. Pressure-dependent (A) absorption and (B) PL spectra of the Au_{21} nanocluster. Solid lines are spectra with increasing pressure. The dotted line is a spectrum taken after pressure was released to 0.22 GPa. Inset in upper figure in (B) is the change in absorption (black square) and PL (red dot) peak wavelength with increasing pressure. Inset in lower figure in (B) is the atomic structure of the Au_{21} nanocluster. Arrows mark the direction of the shift in absorption or PL.

The pressure-dependent absorption and PL of the $Au_{28}(S\text{-}TBBT)_{20}$ nanocluster (Au_{28} for short hereafter) was studied to investigate a *fcc* nanocluster with more metal atoms (**Figure 2**). This nanocluster has a bi-cuboctahedral *fcc* kernel. Under ambient environment, it shows absorption peaks at 480 and 580

nm [24] and PL at ~780 nm.[44] As pressure is increased to ~2 GPa, the near-band-edge absorption increases and red-shifts, while the higher-energy transition at ~480 nm becomes faint. As pressure is further increased to ~5 GPa, the absorption onset red-shifts, and both absorption peaks become faint. The PL intensity is significantly enhanced at elevated pressures up to ~2 GPa. The PL peak red-shifts with increasing pressure up to ~5 GPa, which is similar to the near-band-edge absorption.

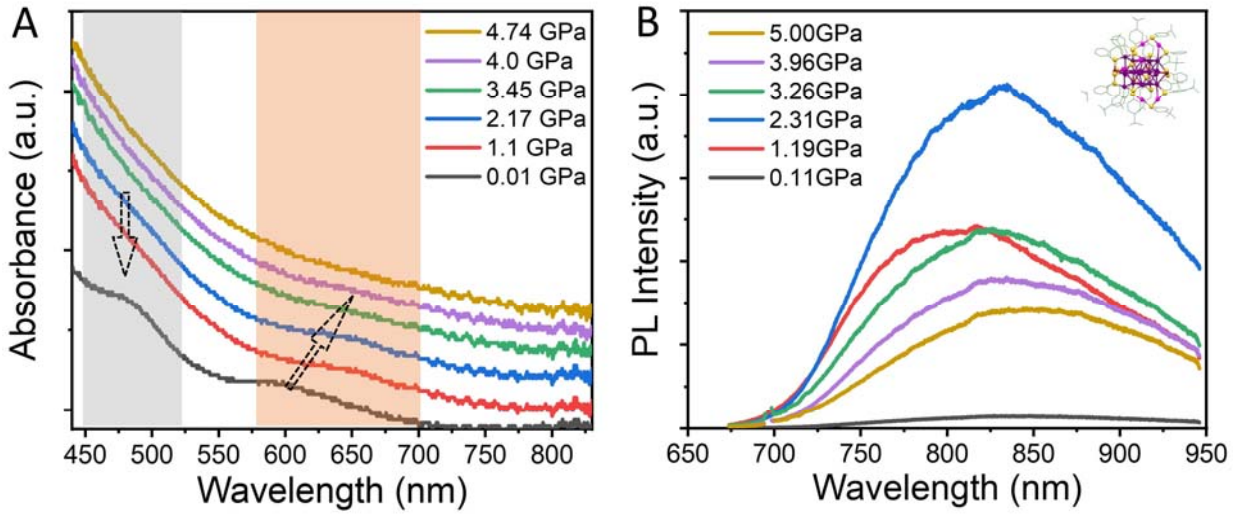

Figure 2. Pressure-dependent (A) absorption and (B) PL of the Au_{28} nanocluster. Inset in (B) is the atomic structure of the Au_{28} nanocluster. Arrows mark the direction of the shift in absorption.

To determine whether the pressure-induced red-shift and activation of the near-band-edge transitions are observed in other bimetallic nanoclusters with *fcc* kernel structures, pressure–dependent optical absorption and PL spectra were obtained for $Ag_{28}Pt_1(S–Adm)_{18}(PPh_3)_4$ ($Ag_{28}Pt_1$ for short hereafter) (**Figure 3)**. At ambient pressures, $Ag_{28}Pt_1$ shows an intense absorption peak at ~450 nm with a long absorption "tail" starting from ~630 nm, and PL centered at ~740 nm (Figure S2). Thus, the Stokes-shift of $Ag_{28}Pt_1$ is as large as 290 nm (1.08eV). Under pressure, the absorption onset gradually red-shifts with increasing pressure (Figure 3A). A new absorption shoulder at ~550 nm gradually becomes significant at ~5 GPa (see Figure S3 for relative intensities of the two absorption peaks). In contrast, the intense absorption peak at ~450 nm slightly blue-shifts and decreases in intensity as pressure increases. These results indicate that the long absorption "tail" at ambient pressure arises from the low oscillator strength of the near-band-edge transition, and that pressure-induced structural changes significantly alter the oscillator strength of the electronic transitions. This leads to the emergence of the near-band-edge transition in the absorption spectrum. At even higher pressures between 5 and 10 GPa, the absorption onset further red-shifts but the absorption peaks become faint. This likely corresponds to a highly distorted nanocluster structure.

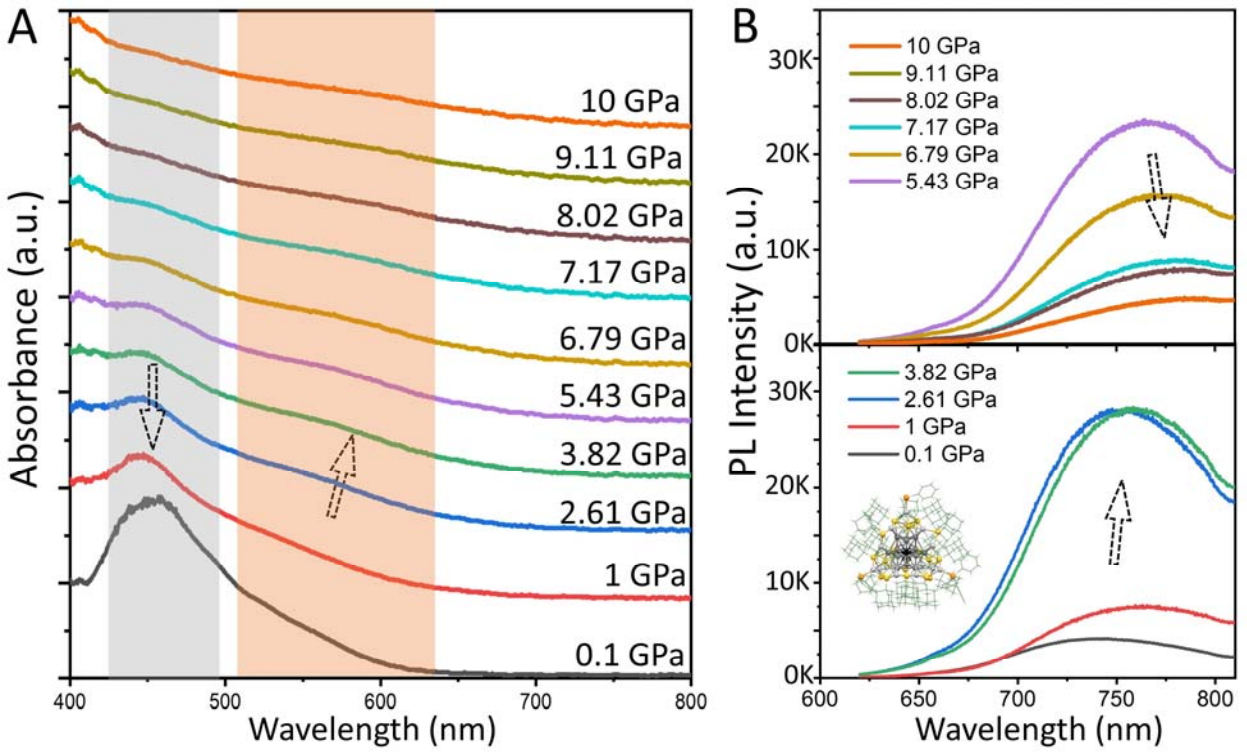

Figure 3. Pressure-dependent (A) absorption and (B) PL of the $Ag_{28}Pt_1(S\text{-}Adm)_{18}(PPh_3)_4$ nanocluster. Inset of (B) is the atomic structure of the $Ag_{28}Pt_1$ nanocluster. Arrows mark the direction of the shift in absorption or PL.

High-pressure PL spectra of $Ag_{28}Pt_1$ are shown in Figure 3B. The PL red-shifts from 740 nm to 780 nm as pressure is increased to 10 GPa. Meanwhile, the PL intensity is significantly (~6 times) enhanced by an increase in pressure to 5 GPa, but then decreases as the pressure is further increased to 10 GPa. The increase in wavelength and intensity of both the PL and near-band-edge absorption under pressure indicates that PL and absorption arise from the same electronic states, while the intense absorption at 460 nm is likely to have a different structural origin. This provides insight into the origin of the observed PL in nanoclusters and the mechanism behind the large observed Stokes-shift in ambient environment. In previous studies, state-transition models such as intersystem crossing[45] and charge transfer[46] have been proposed to explain the large Stokes shift observed in metal nanoclusters. Our results show that the apparent large Stokes shift in the $Ag_{28}Pt_1$ nanocluster (between the absorption peak at ~450 nm and the PL at ~740 nm) is not the actual Stokes shift because this absorption peak is not responsible for the PL. Instead, the Stokes shift should be measured at the absorption peak that emerges under high pressure. Under ambient environment, this neglected absorption band does not appear due to its very low oscillator strength. By increasing pressure, the oscillator strength of these low-energy transitions is enhanced due to the distortion of the atomic structure. Thus, the transitions become observable in the high-pressure absorption spectra and the PL becomes enhanced. With this understanding of the near-band-edge

transition (*e.g.* HOMO-LUMO), the actual Stokes-shift is found to be much smaller, which indicates that the excited-state transition may not exist in $Ag_{28}Pt_1$. Additionally, the PL of $Ag_{28}Pt$ does not change in different solvents (Figure S4). This suggests that significant charge-transfer effects do not exist in this nanocluster.

In summary, all of the *fcc* nanoclusters studied here (mono-cuboctahedral $Ag_{28}Pt_1$ and Au_{21} nanoclusters, and the bi-cuboctahedral Au_{28} nanocluster) exhibit a red-shift in absorption and an up to 20-fold enhancement in PL intensity under pressure. This indicates that these optical changes are a general phenomenon for the ultrasmall *fcc* gold and silver nanoclusters. We also consider the influence of the pressure medium on optical changes. The nanoclusters were compressed by using toluene as a pressure medium. Toluene is a hydrostatic pressure medium below its freezing point of ~2 GPa, and a non-hydrostatic pressure medium above this pressure.[47,48] To test the effect of non-hydrostaticity on optical transitions, we performed high-pressure measurements using chloroform as the pressure medium. As shown in Figure S5, the pressure-dependent changes of absorption and PL are almost the same as they are in toluene, except for a sudden blue-shift at ~3 GPa which corresponds to a phase transition of solid chloroform. The quasi-hydrostatic pressure medium 4:1 methanol/ethanol was also tested on an Au_{21}-assembled single crystal, and the pressure-dependent red-shift of PL(Figure S6) was found to be the same as for toluene (note: Au_{21} nanoclusters cannot be dissolved in methanol/ethanol so absorption under hydrostatic compression could not be measured). These results suggest that changes in absorption and PL are due to structural compression caused by pressure, rather than the nature of the pressure medium or solvation effects. Additionally, optical changes are similar under non-hydrostatic and hydrostatic compression.

Density functional theory calculations

Ground-state and time-dependent DFT calculations were performed to understand the effect of pressure on electronic transitions within the nanoclusters. The Au_{21} nanocluster was chosen as a representative *fcc* nanocluster for DFT calculations. Calculations were carried out at 0, 4.5, 9.9, 12, and 14 GPa. From these calculations, we constructed isolated models of the clusters by replacing the ligands by methyl substituents; this allows us to focus on the metal core and nearby S and P atoms, and reduce computational costs (Figure S7). These clusters were then analyzed with linear-response TDDFT. **Fig 4A** shows the absorption spectra for several pressures. In agreement with the experimental observations, we note that the spectrum indeed red-shifts. This is noticeable, for example, by comparing the curves for 0 and 4.5 GPa, where the absorption onset red-shifts from about ~680 nm to 780 nm. This shift continues as the pressure is further increased, although the computed spectra for 9.9 and 12 GPa look similar. In addition, we also performed DFT calculations to study $Ag_{28}Pt_1$ under high pressures and the absorptions show a similar red-shifting trend under increasing pressures (Figure S8).

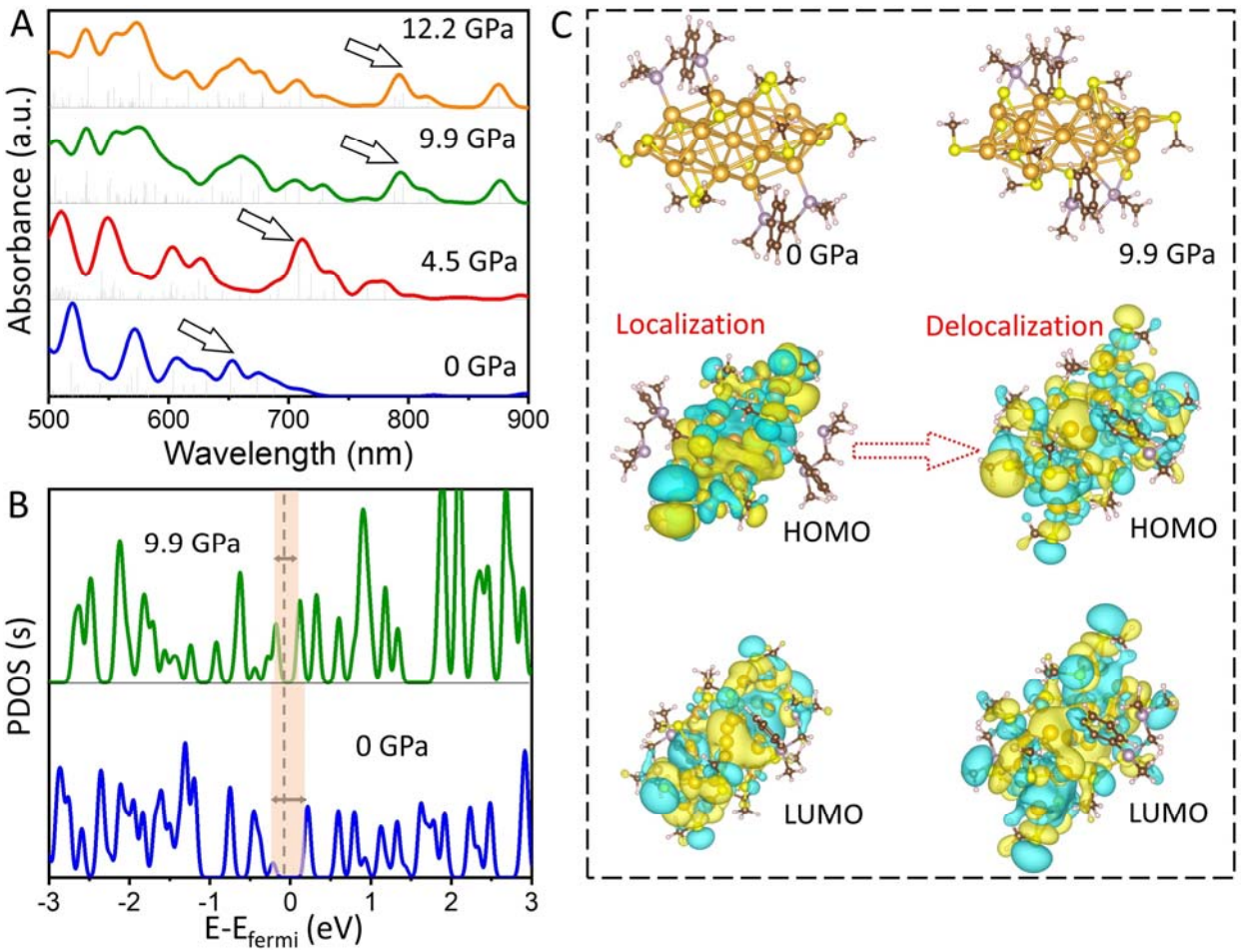

Figure 4. DFT calculations of Au_{21} electronic structure. (A) Computed absorption spectrum of an isolated Au_{21} nanocluster. The arrows indicate the major near-band-edge absorption. (B) Density of Au *s*-states as a function of pressure at 0 and 9.9 GPa. (C) Atomic structures and orbital diagrams for Au_{21} at 0 GPa (Left) and 9.9 GPa (Right). The dominant underlying transition for the main absorption peaks (arrow) are shown in Table S1.

To understand the red-shifts in the calculated spectra, we computed the principal normalized inertia moments of the clusters and note that the shape of the cluster remains prolate with increasing pressure (Figure S9). This indicates that shape change is not the reason for the differences in optical spectra. Another effect is the change in bond distances. It is calculated from Figure S9 that the average bond distance between the Au atoms of the surface Au_3S_4 motif and the Au atoms in the kernel decreases by ~0.02 and 0.06 Å with increase in pressure from 0 to 4.5 GPa and 9.9 GPa, respectively. The phosphine-based carbon ligands also move closer to the gold kernel as pressure increases. Under ambient conditions, the HOMO electrons are mainly localized in the cuboctahedral metal kernel, within the core of the Au_{21} (Figure 4C) (as is also the case for other *fcc* nanoclusters[44,49]) which leads to an electronic "separation" of the outer atoms from the kernel Au. Intuitively, one might expect that as pressure is increased, and the ligands move toward the core, there would be increased quantum confinement in the core, leading to

larger band gaps and blue-shifted spectra. However, the computational results indicate that the opposite occurs, with the projected density–of–states (PDOS) showing a significant narrowing of the energy level spacing, as can be seen in Figure 4B (and Figure S10 and S11 for other energy levels). To explain this, we have examined frontier orbitals (Figure 4C) and other orbitals that are important in the spectra (Figures S12 and S13). These clearly show increased electron delocalization with increased pressure. In addition, we computed the atomic orbital contributions to molecular orbitals (Table S1) that are involved in the prominent absorption bands (arrow, Figure 4A) for the Au_{21} cluster with trimmed ligands. Our analysis shows that the underlying transitions for the main observed absorption peaks (arrow, Figure 4A) of Au_{21} change under different pressures, but maintain an "interband" d-to-s transition character (Table S1). The transition strength of these main absorptions increases with the pressure up to 4.5 GPa and then decreases as the pressure further goes up to 9 and 12 GPa, which is similar to the pressure-dependence of PL intensity observed in experiment. All these transitions involve the ligands, and even more so as the pressure increases. Although the sulfur atoms, which are covalently bound to the gold core of the nanocluster, lose electron population as pressure is increased, the phosphorus and carbon atoms of the ligands gain population, with P and C atoms increasing from 4 to 8%, and even up to 17% (Table S1). Hence, exerting pressure on the system induces delocalization of the electron density to the ligands, increasing the size of the box available to the electrons, and thereby narrowing of the energy level spacing. These observations correlate with the computed red-shifting behavior.

Bi-tetrahedral nanoclusters

To investigate whether the pressure-induced red-shift of band-edge absorption and enhancement of PL can be observed in other metal nanoclusters, we conducted high-pressure studies on two bi-tetrahedral nanoclusters: $Au_{24}(S\text{-}TBBM)_{20}$[41] (S-TBBM=4-tertbutylphenylmethancan, Au_{24} for short hereafter) and $Au_{14}Cd_1(S\text{-}Adm)_{12}$[42] (S-Adm = 1-adamantanethiol, $Au_{14}Cd$ for short hereafter). As shown in Figure 5, the absorption of the two bi-tetrahedral nanoclusters shows a similar red-shift with increasing pressure. Significant enhancement of PL is also observed for these two nanoclusters. Of note, there is a ~200-fold enhancement of the PL intensity for $Au_{14}Cd$. Different from the previous *fcc* nanoclusters, the PL of the two bi-tetrahedral nanoclusters first slightly blue-shifts as the pressure is increased from 0 to ~3 GPa. Such pressure-induced blue-shift can be ascribed to the suppression of the excited-state structural-distortion to a second low-energy and low-efficiency state which induces another redder PL overlapping with the main PL peak under ambient pressures[50] (more details in the ref 50). This mechanism of pressure-induced enhancement of PL in bi-tetrahedral nanoclusters (*i.e.* hinderance of excited-state structural distortion) is different from the previous *fcc* series of nanoclusters. As the pressure is increased above ~ 3 GPa, the PL of these two bi-tetrahedral nanoclusters red-shifts and further increases in intensity

(up to 4.8 GPa for Au_{24} in toluene and up to 7.45 GPa for $Au_{14}Cd$ in ethylcyclohexane), which is similar to the previous *fcc* series of nanoclusters.

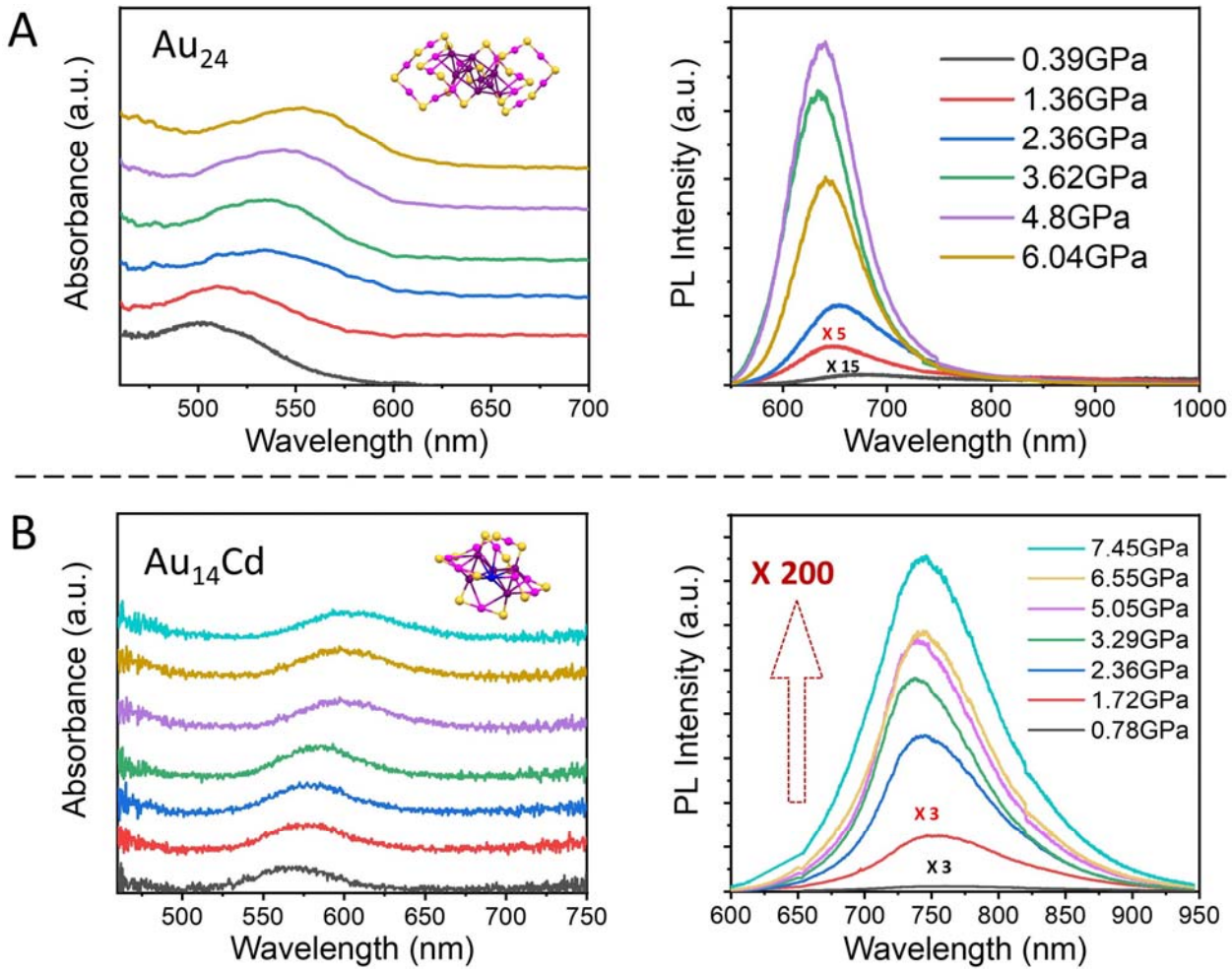

Figure 5. Pressure dependent absorption (left) and PL (right) for A) $Au_{24}(S\text{-}TBBM)_{20}$ and B) $Au_{14}Cd_1(S\text{-}Adm)_{12}$. In each panel, the pressure-dependent absorption spectra are shown on the left and the pressure-dependent PL spectra on the right. Insets are the atomic structures of the Au_{24} and $Au_{14}Cd$ nanoclusters. The PL data of Au_{24} below 3.62 GPa are from ref 50.

It can be observed from Figure 5 that from 0 to ~6 GPa, the absorption peak of $Au_{14}Cd$ red-shifts by ~25 nm, while Au_{24} red-shifts by ~55 nm. These two nanoclusters differ in their ligands; $Au_{14}Cd$ has aliphatic ligands, while Au_{24} has aromatic ligands that contain phenyl rings. We propose that the compression of these aromatic ligands to high pressures leads to more electron delocalization, which leads to the larger red-shift. This result brings up the possibility of tuning the pressure sensitivity of the nanoclusters by changing the ligand environment. DFT simulations were also conducted on the $Au_{14}Cd$ nanocluster. Calculations were carried out at 0, 3.5 and 7 GPa (Figure S14). In agreement with the experimental observations, we note that the calculated absorption spectrum indeed slightly red-shifts with the pressure up to 7 GPa (Figure S14). The absorption peak intensity does not change significantly with

pressure in either experimental or simulated results. This indicates that the transition dipole is not enhanced at high pressure. Thus, the dramatic pressure-induced enhancement of the PL in $Au_{14}Cd$ should be ascribed to the suppression of the excited-state non-radiative processes (*i.e*. structural distortions and vibrations).

Conclusions.

A systematic high-pressure optical study has been conducted on a series of *fcc* and bi-tetrahedral nanoclusters. Red-shifts of the absorption onset under high pressures were identified in all the nanocluster samples. DFT results suggest the pressure-induced red-shift in absorption arises from electron delocalization to the ligands when the nanocluster is squeezed. Furthermore, up to 200-fold enhancement of the PL intensity has been realized with increase in pressure up to ~7 GPa. The pressure-induced PL enhancement is ascribed to i) the enhancement of the near-band-edge transition dipole, ii) suppression of the non-radiative vibrations and ii) hinderance of the excited-state structural distortion. This work shows that the high-pressure method can indeed deepen our understanding of the electronic structure and tune the optical properties of nanoclusters. Furthermore, our results also suggest the high-pressure can be used as an effective and general tool to enhance the PL brightness of different ultrasmall nanoclusters.

Methods and Materials.

Synthesis. The $Ag_{28}Pt_1$, Au_{21}, Au_{28}, Au_{24} and $Au_{14}Cd$ nanocluster samples were synthesized and crystallized following previously reported methods.[23–25,41,42]

Diamond anvil cell compression. Two identical diamond anvils with a culet of 500 μm were used to generate pressure. A 200 to 300 μm diameter hole was drilled hole in a stainless-steel gasket to serve as the sample chamber. Toluene, chloroform, ethylcyclohexane and methanol/ethanol (4:1) were used as pressure mediums. Ruby spheres were loaded alongside the samples and used to calibrate the pressure by the fluorescent technique.

In situ **high-pressure absorption and PL measurements.** Absorption measurements were taken on a home-built Nikon microscope system using 10X objective. For the absorption measurements, a halogen lamp (15 V, 150 W, 3100 K) was chosen as the white light source. The Flame Detector 200-1000 nm (Ocean Optics, Inc) was used as the detector. PL spectra were measured using this Nikon microscope system and the Horiba XploRA+ Confocal Raman setup using 10X objective. Samples were excited by a 532 nm laser and the fluorescent signal was collected using a 600 gr/mm diffraction grating.

Theoretical calculations. To compute the structural changes of the clusters due to pressure, DFT geometry optimizations (including variable cell) and PDOS were performed with the program SIESTA

(Spanish Initiative for Electronic Simulations with Thousands of Atoms, version 4.1-b4).[51] The exchange-correlation functional for these calculations is the PBE GGA. The Au_{21} cluster was reproduced using the experimental unit cell at normal pressure. The basis set for all the atoms is SZP, except Au for the DZP basis. The energy cut-off to generate the basis set is the standard value, 20 Ry, while the 300 Ry was chosen as the cut-off energy value for the mesh plane waves (this value renders "eggbox" effects negligible). The density matrix threshold for the self-consistent cycles is 1×10^{-5}, the tolerance value for the geometry relaxation is 0.05 eV/Å, and for the unit-cell optimization we use 0.15 GPa. The Au_{21} cluster was computed at 0 GPa, 4.5 Gpa, 9.9 GPa, 12 GPa, and 14 GPa. For the PDOS calculations we extracted the single cluster of interest from the unit cells and 'trimmed' the ligands to reduce the size of the molecule as shown in Figure S11. The absorption spectra of these clusters were also studied with linear-response time-dependent DFT in the program ORCA and with the functional BP86.[52] The Tamm-Dancoff and a Davidson threshold of 1×10^{-5} were used for these calculations.

Supporting Information

The Supporting Information is available free of charge online.

The Supporting Information contains additional pressure-dependent spectra, ambient absorption and PL spectra, and additional DFT results, including the DOS, frontier orbitals and orbital contribution to the underlying transitions in the metal nanoclusters.

Acknowledgements. Q.L., X.W.G., M.A.M. and G.C.S acknowledge National Science Foundation (NSF) grant DMR-2002936/2002891. Part of this work was performed at the Stanford Nano Shared Facilities (SNSF), which is supported by the National Science Foundation under award ECCS-1542152. MAM, LOJ and GCS were supported by DOE grant DE-AC02-06CH11357 for theory development. This research was supported in part through the computational resources and staff contributions provided for the Quest high performance computing facility at Northwestern University which is jointly supported by the Office of the Provost, the Office for Research, and Northwestern University Information Technology. Part of this work was performed at the Stanford Nano Shared Facilities (SNSF), supported by the National Science Foundation under Grant No. ECCS-1542152.

References

(1) Jin, R.; Zeng, C.; Zhou, M.; Chen, Y. Atomically Precise Colloidal Metal Nanoclusters and Nanoparticles: Fundamentals and Opportunities. *Chem. Rev.* **2016**, *116*, 10346–10413.

(2) Zeng, C.; Chen, Y.; Kirschbaum, K.; Appavoo, K.; Sfeir, M. Y.; Jin, R. Structural Patterns at All Scales in a Nonmetallic Chiral Au133(SR)52 Nanoparticle. *Sci. Adv.* **2015**, *1*, e1500045.

(3) Aikens, C. M. Electronic and Geometric Structure, Optical Properties, and Excited State Behavior in Atomically Precise Thiolate-Stabilized Noble Metal Nanoclusters. *Acc. Chem. Res.* **2018**, *51*, 3065–3073.
(4) Zhu, M.; Aikens, C. M.; Hollander, F. J.; Schatz, G. C.; Jin, R. Correlating the Crystal Structure of A Thiol-Protected Au25 Cluster and Optical Properties. *J. Am. Chem. Soc.* **2008**, *130*, 5883–5885.
(5) Zeng, C.; Qian, H.; Li, T.; Li, G.; Rosi, N. L.; Yoon, B.; Barnett, R. N.; Whetten, R. L.; Landman, U.; Jin, R. Total Structure and Electronic Properties of the Gold Nanocrystal Au36(SR)24. *Angew. Chem.* **2012**, *124*, 13291–13295.
(6) Chen, S. Gold Nanoelectrodes of Varied Size: Transition to Molecule-Like Charging. *Science* **1998**, *280*, 2098–2101.
(7) Walter, M.; Akola, J.; Lopez-Acevedo, O.; Jadzinsky, P. D.; Calero, G.; Ackerson, C. J.; Whetten, R. L.; Grönbeck, H.; Häkkinen, H. A Unified View of Ligand-Protected Gold Clusters as Superatom Complexes. *Proc. Natl. Acad. Sci.* **2008**, *105*, 9157–9162.
(8) Yang, H.; Wang, Y.; Chen, X.; Zhao, X.; Gu, L.; Huang, H.; Yan, J.; Xu, C.; Li, G.; Wu, J.; Edwards, A. J.; Dittrich, B.; Tang, Z.; Wang, D.; Lehtovaara, L.; Häkkinen, H.; Zheng, N. Plasmonic Twinned Silver Nanoparticles with Molecular Precision. *Nat. Commun.* **2016**, *7*, 1–8.
(9) Bakr, O. M.; Amendola, V.; Aikens, C. M.; Wenseleers, W.; Li, R.; Dal Negro, L.; Schatz, G. C.; Stellacci, F. Silver Nanoparticles with Broad Multiband Linear Optical Absorption. *Angew. Chem. Int. Ed.* **2009**, *48*, 5921–5926.
(10) Bigioni, T. P.; Whetten, R. L.; Dag, Ö. Near-Infrared Luminescence from Small Gold Nanocrystals. *J. Phys. Chem. B* **2000**, *104*, 6983–6986.
(11) Li, Q.; Zhou, M.; So, W. Y.; Huang, J.; Li, M.; Kauffman, D. R.; Cotlet, M.; Higaki, T.; Peteanu, L. A.; Shao, Z.; Jin, R. A Mono-Cuboctahedral Series of Gold Nanoclusters: Photoluminescence Origin, Large Enhancement, Wide Tunability, and Structure–Property Correlation. *J. Am. Chem. Soc.* **2019**, *141*, 5314–5325.
(12) Wang, G.; Huang, T.; Murray, R. W.; Menard, L.; Nuzzo, R. G. Near-IR Luminescence of Monolayer-Protected Metal Clusters. *J. Am. Chem. Soc.* **2005**, *127*, 812–813.
(13) Xie, J.; Zheng, Y.; Ying, J. Y. Protein-Directed Synthesis of Highly Fluorescent Gold Nanoclusters. *J. Am. Chem. Soc.* **2009**, *131*, 888–889.
(14) Wang, S.; Meng, X.; Das, A.; Li, T.; Song, Y.; Cao, T.; Zhu, X.; Zhu, M.; Jin, R. A 200-Fold Quantum Yield Boost in the Photoluminescence of Silver-Doped AgxAu25−x Nanoclusters: The 13 Th Silver Atom Matters. *Angew. Chem. Int. Ed.* **2014**, *53*, 2376–2380.
(15) Kelly, K. L.; Coronado, E.; Zhao, L. L.; Schatz, G. C. The Optical Properties of Metal Nanoparticles: The Influence of Size, Shape, and Dielectric Environment. *J. Phys. Chem. B* **2003**, *107*, 668–677.
(16) Hartland, G. V. Optical Studies of Dynamics in Noble Metal Nanostructures. *Chem. Rev.* **2011**, *111* (6), 3858–3887.
(17) Negishi, Y.; Takasugi, Y.; Sato, S.; Yao, H.; Kimura, K.; Tsukuda, T. Magic-Numbered Aun Clusters Protected by Glutathione Monolayers (n = 18, 21, 25, 28, 32, 39): Isolation and Spectroscopic Characterization. *J. Am. Chem. Soc.* **2004**, *126*, 6518–6519.
(18) Jadzinsky, P. D.; Calero, G.; Ackerson, C. J.; Bushnell, D. A.; Kornberg, R. D. Structure of a Thiol Monolayer-Protected Gold Nanoparticle at 1.1 Å Resolution. *Science* **2007**, *318*, 430–433.
(19) Chakraborty, I.; Pradeep, T. Atomically Precise Clusters of Noble Metals: Emerging Link between Atoms and Nanoparticles. *Chem. Rev.* **2017**, *117*, 8208–8271.
(20) Yan, N.; Xia, N.; Liao, L.; Zhu, M.; Jin, F.; Jin, R.; Wu, Z. Unraveling the Long-Pursued Au144 Structure by x-Ray Crystallography. *Sci. Adv.* **2018**, *4*, eaat7259.
(21) Zeng, C.; Chen, Y.; Kirschbaum, K.; Lambright, K. J.; Jin, R. Emergence of Hierarchical Structural Complexities in Nanoparticles and Their Assembly. *Science* **2016**, *354*, 1580–1584.
(22) Yau, S. H.; Ashenfelter, B. A.; Desireddy, A.; Ashwell, A. P.; Varnavski, O.; Schatz, G. C.; Bigioni, T. P.; Goodson, T. Optical Properties and Structural Relationships of the Silver Nanoclusters Ag32(SG)19 and Ag15(SG)11. *J. Phys. Chem. C* **2017**, *121*, 1349–1361.

(23) Lin, X.; Liu, C.; Sun, K.; Wu, R.; Fu, X.; Huang, J. Structural Isomer and High-Yield of Pt1Ag28 Nanocluster *via* One-Pot Chemical Wet Method. *Nano Res.* **2019**, *12*, 309–314.
(24) Zeng, C.; Li, T.; Das, A.; Rosi, N. L.; Jin, R. Chiral Structure of Thiolate-Protected 28-Gold-Atom Nanocluster Determined by X-Ray Crystallography. *J. Am. Chem. Soc.* **2013**, *135*, 10011–10013.
(25) Li, Q.; Luo, T.-Y.; Taylor, M. G.; Wang, S.; Zhu, X.; Song, Y.; Mpourmpakis, G.; Rosi, N. L.; Jin, R. Molecular "Surgery" on a 23-Gold-Atom Nanoparticle. *Sci. Adv.* **2017**, *3*, e1603193..
(26) Li, Q.; Lambright, K. J.; Taylor, M. G.; Kirschbaum, K.; Luo, T.-Y.; Zhao, J.; Mpourmpakis, G.; Mokashi-Punekar, S.; Rosi, N. L.; Jin, R. Reconstructing the Surface of Gold Nanoclusters by Cadmium Doping. *J. Am. Chem. Soc.* **2017**, *139*, 17779–17782.
(27) Zhang, L.; Wang, Y.; Lv, J.; Ma, Y. Materials Discovery at High Pressures. *Nat. Rev. Mater.* **2017**, *2*, 17005.
(28) Mao, H.-K.; Chen, X.-J.; Ding, Y.; Li, B.; Wang, L. Solids, Liquids, and Gases under High Pressure. *Rev. Mod. Phys.* **2018**, *90*, 015007.
(29) Hannah, D. C.; Yang, J.; Podsiadlo, P.; Chan, M. K. Y.; Demortière, A.; Gosztola, D. J.; Prakapenka, V. B.; Schatz, G. C.; Kortshagen, U.; Schaller, R. D. On the Origin of Photoluminescence in Silicon Nanocrystals: Pressure-Dependent Structural and Optical Studies. *Nano Lett.* **2012**, *12*, 4200–4205.
(30) Welber, B.; Kim, C. K.; Cardona, M.; Rodriguez, S. Dependence of the Indirect Energy Gap of Silicon on Hydrostatic Pressure. *Solid State Commun.* **1975**, *17*, 1021–1024.
(31) Nayak, A. P.; Yuan, Z.; Cao, B.; Liu, J.; Wu, J.; Moran, S. T.; Li, T.; Akinwande, D.; Jin, C.; Lin, J.-F. Pressure-Modulated Conductivity, Carrier Density, and Mobility of Multilayered Tungsten Disulfide. *ACS Nano* **2015**, *9*, 9117–9123.
(32) Chauvin, N.; Mavel, A.; Patriarche, G.; Masenelli, B.; Gendry, M.; Machon, D. Pressure-Dependent Photoluminescence Study of Wurtzite InP Nanowires. *Nano Lett.* **2016**, *16*, 2926–2930.
(33) Nagaoka, Y.; Hills-Kimball, K.; Tan, R.; Li, R.; Wang, Z.; Chen, O. Nanocube Superlattices of Cesium Lead Bromide Perovskites and Pressure-Induced Phase Transformations at Atomic and Mesoscale Levels. *Adv. Mater.* **2017**, *29*, 1606666.
(34) Jaffe, A.; Lin, Y.; Beavers, C. M.; Voss, J.; Mao, W. L.; Karunadasa, H. I. High-Pressure Single-Crystal Structures of 3D Lead-Halide Hybrid Perovskites and Pressure Effects on Their Electronic and Optical Properties. *ACS Cent. Sci.* **2016**, *2*, 201–209.
(35) Li, Q.; Chen, Z.; Yang, B.; Tan, L.; Xu, B.; Han, J.; Zhao, Y.; Tang, J.; Quan, Z. Pressure-Induced Remarkable Enhancement of Self-Trapped Exciton Emission in One-Dimensional CsCu2I3 with Tetrahedral Units. *J. Am. Chem. Soc.* **2020**, *142*, 1786–1791.
(36) Xiao, G.; Cao, Y.; Qi, G.; Wang, L.; Liu, C.; Ma, Z.; Yang, X.; Sui, Y.; Zheng, W.; Zou, B. Pressure Effects on Structure and Optical Properties in Cesium Lead Bromide Perovskite Nanocrystals. *J. Am. Chem. Soc.* **2017**, *139*, 10087–10094.
(37) Gu, X. W.; Hanson, L. A.; Eisler, C. N.; Koc, M. A.; Alivisatos, A. P. Pseudoelasticity at Large Strains in Au Nanocrystals. *Phys. Rev. Lett.* **2018**, *121*, 056102.
(38) Martín-Sánchez, C.; Barreda-Argüeso, J. A.; Seibt, S.; Mulvaney, P.; Rodríguez, F. Effects of Hydrostatic Pressure on the Surface Plasmon Resonance of Gold Nanocrystals. *ACS Nano* **2019**, *13*, 498–504.
(39) Li, Q.; Niu, W.; Liu, X.; Chen, Y.; Wu, X.; Wen, X.; Wang, Z.; Zhang, H.; Quan, Z. Pressure-Induced Phase Engineering of Gold Nanostructures. *J. Am. Chem. Soc.* **2018**, *140*, 15783–15790.
(40) Medeghini, F.; Hettich, M.; Rouxel, R.; Silva Santos, S. D.; Hermelin, S.; Pertreux, E.; Torres Dias, A.; Legrand, F.; Maioli, P.; Crut, A.; Vallée, F.; San Miguel, A.; Del Fatti, N. High-Pressure Effect on the Optical Extinction of a Single Gold Nanoparticle. *ACS Nano* **2018**, *12*, 10310–10316.
(41) Das, A.; Li, T.; Li, G.; Nobusada, K.; Zeng, C.; Rosi, N. L.; Jin, R. Crystal Structure and Electronic Properties of a Thiolate-Protected Au24 Nanocluster. *Nanoscale* **2014**, *6*, 6458–6462.
(42) Yang, S.; Chen, S.; Xiong, L.; Liu, C.; Yu, H.; Wang, S.; Rosi, N. L.; Pei, Y.; Zhu, M. Total Structure Determination of Au16(S-Adm)12 and Cd1Au14(StBu)12 and Implications for the Structure of Au15(SR)13. *J. Am. Chem. Soc.* **2018**, *140*, 10988–10994.

(43) Herbst, C. A.; Cook, R. L.; King, H. E. Density-Mediated Transport and the Glass Transition: High Pressure Viscosity Measurements in the Diamond Anvil Cell. *J. Non-Cryst. Solids* **1994**, *172–174*, 265–271.
(44) Zhou, M.; Zeng, C.; Sfeir, M. Y.; Cotlet, M.; Iida, K.; Nobusada, K.; Jin, R. Evolution of Excited-State Dynamics in Periodic Au28, Au36, Au44, and Au52 Nanoclusters. *J. Phys. Chem. Lett.* **2017**, *8*, 4023–4030.
(45) Sugiuchi, M.; Maeba, J.; Okubo, N.; Iwamura, M.; Nozaki, K.; Konishi, K. Aggregation-Induced Fluorescence-to-Phosphorescence Switching of Molecular Gold Clusters. *J. Am. Chem. Soc.* **2017**, *139*, 17731–17734.
(46) Wu, Z.; Liu, H.; Li, T.; Liu, J.; Yin, J.; Mohammed, O. F.; Bakr, O. M.; Liu, Y.; Yang, B.; Zhang, H. Contribution of Metal Defects in the Assembly Induced Emission of Cu Nanoclusters. *J. Am. Chem. Soc.* **2017**, *139*, 4318–4321.
(47) Gu, X. W.; Hanson, L. A.; Eisler, C. N.; Koc, M. A.; Alivisatos, A. P. Pseudoelasticity at Large Strains in Au Nanocrystals. *Phys. Rev. Lett.* **2018**, *121*, 056102.
(48) Parakh, A.; Lee, S.; Harkins, K. A.; Kiani, M. T.; Doan, D.; Kunz, M.; Doran, A.; Hanson, L. A.; Ryu, S.; Gu, X. W. Nucleation of Dislocations in 3.9 Nm Nanocrystals at High Pressure. *Phys. Rev. Lett.* **2020**, *124*, 106104.
(49) Das, A.; Li, T.; Nobusada, K.; Zeng, C.; Rosi, N. L.; Jin, R. Nonsuperatomic [Au23(SC6H11)16]− Nanocluster Featuring Bipyramidal Au15 Kernel and Trimeric Au3(SR)4 Motif. *J. Am. Chem. Soc.* **2013**, *135*, 18264–18267.
(50) Li, Q.; Zhou, D.; Chai, J.; So, W. Y.; Cai, T.; Li, M.; Peteanu, L. A.; Chen, O.; Cotlet, M.; Wendy Gu, X.; Zhu, H.; Jin, R. Structural Distortion and Electron Redistribution in Dual-Emitting Gold Nanoclusters. *Nat. Commun.* **2020**, *11*, 2897.
(51) Soler, J. M.; Artacho, E.; Gale, J. D.; García, A.; Junquera, J.; Ordejón, P.; Sánchez-Portal, D. The SIESTA Method For *Ab Initio* order-Nmaterials Simulation. *J. Phys. Condens. Matter* **2002**, *14*, 2745–2779.
(52) Neese, F. Software Update: The ORCA Program System, Version 4.0. *Wiley Interdiscip. Rev. Comput. Mol. Sci.* **2018**, *8*, e1327.

TOC

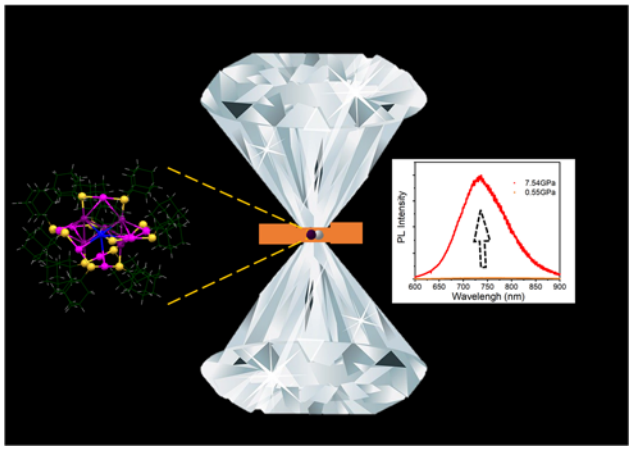

For Table of Contents Only